A Modeling Framework and Flux Controller for Free Molecular Flow Deposition Processes

Dresscher, Martijn; Jayawardhana, Bayu; Barradas Berglind, Jose de Jesus; Scherpen, Jacquelien M.A.

Published in:
Proceedings of the American Control Conference

DOI:
10.23919/ACC.2017.7963273

Publication date:
2017

A Modeling Framework and Flux Controller for Free Molecular Flow Deposition Processes

M. Dresscher, B. Jayawardhana, J.J. Barradas-Berglind & J.M.A. Scherpen

***Abstract*— In this paper, we introduce a modeling framework for free molecular flow (FMF) processes (such as, deposition processes under an ultra-high vacuum condition) that is suitable for model-based control design. The generic dynamical model is comprised of four important elements in such processes: (i) particle transfer, which is modeled based on the well-known Knudsen cosine law; (ii) particle leakage; (iii) adsorption and desorption described by a (nonlinear) sticking function; and (iv) control input particle flux. As a starting point for obtaining accurate control on the deposition process in FMF regime, we propose a control design method for stabilization with guaranteed transient behavior for fluxes. It is based on a point-wise min-norm control approach, employing both control Lyapunov and control barrier functions. Lastly, we validate our model, applied to a cylindrical geometry, with existing results in literature and evaluate the effectiveness of the proposed control method for controlling the fluxes.**

I. Introduction

Modeling of free molecular flow (FMF) started in the early 20*th* century with a series of experiments performed by Knudsen. In his first paper in 1909 [1], Knudsen introduced two fundamental concepts: (i) a defining criterion for FMF, now known as the Knudsen number, and (ii) the first arguments for the validity of a cosine law for diffusion from rough surfaces, thus becoming the so-called Knudsen cosine law. Knudsen formally introduced this cosine law in kinetic theory in 1915 [2]. During the following 75 years, many useful contributions were made based on these fundamental insights. The history of FMF theory was nicely documented in the 1986 review by Steckelmacher [3]. Since then, modeling and simulation methods have been developed to predict the evolution of FMF in industrial processes. A mathematical framework was introduced by Cale and Raupp for simple geometries, such as cylinders [4]. However, for more complex geometries, Monte-Carlo analysis is often performed [5]. Some examples of applications are atomic layer deposition [6], [7], etching [8], isotope separation [9], hydrogen extraction [10], and membrane distillation [11]. More recently, free molecular flow through a capillary was reviewed in [12], and theoretical and simulation approaches were reviewed in [13].

From a control perspective, deposition control in FMF is of interest for specific Chemical Vapor Deposition (CVD) processes such as Ultra-High Vacuum CVD (UHV CVD) and Atomic Layer Deposition (ALD). Where in the latter, the FMF regime is often present in micro-scale trenches. Both processes are used for deposition of thin layers, usually for semi-conductor or other microelectronics manufacturing; an overview of the modeling and control challenges in microelectronics manufacturing can be found in [14]. This paper highlights the challenges with real-time control in such processes due to restrictions on sensor placement, where state estimation gains importance. The state estimation can in turn be combined with reference generation and tracking, through a controllable input and observable (possibly *ex-situ*) output. A series of papers by Holmqvist *et al.* [7], [15], [16] presents a modeling framework for ALD and applies these principles to find optimal operation policies.

In this paper, we implement model-based control with guaranteed performance for fluxes in a FMF regime evolving in a cylindrical geometry. The main contributions of the paper are: (i) the introduction of a FMF modeling framework for controller design; (ii) the corresponding derivation of the scattering dynamics of particles based on the fundamental Knudsen cosine law; and (iii) the implementation of state-of-the-art control for stabilization with guaranteed transient behavior for fluxes in a FMF process under a saturated boundary assumption.

The remainder of the paper is structured as follows. In Section II, we address free molecular flow processes more extensively. Then, in Section III we elaborate on the proposed modeling framework for control and we discuss the different options to derive the dynamics. Subsequently, in Section IV, we present the notion of safety in the context of guaranteed transient behavior, which is instrumental to formulate the control problem of interest. In Section V, we validate the modeling framework described in Section III with results from literature. Moreover, we illustrate the applicability of the control strategy presented in Section IV to stabilize fluxes at a desired equilibrium, while guaranteeing desired transient behavior. Finally, conclusions are presented in Section VI.

II. Preliminary on Free Molecular Flow

FMF is a particle transport regime in environments that have a very large Knudsen number ($\gg 1$). The Knudsen number is defined as the mean free path of a particle divided by a relevant length scale of travel [1]. In free molecular flow, gas phase collisions occur so rarely that gas dynamics are dictated by the solid boundaries. Particularly, the angular distribution of departing particles is of interest, since such distribution in combination with the boundary geometry can

The work of B. Jayawardhana & J.M.A. Scherpen is supported by the national Dutch project on Region of Smart Factories (RoSF).

M. Dresscher, B. Jayawardhana, J.J. Barradas-Berglind and J.M.A. Scherpen are with the Engineering and Technology Institute Groningen (ENTEG), Faculty of Mathematics and Natural Sciences. University of Groningen, Nijenborgh 4, 9747AG Groningen, The Netherlands (m.dresscher@rug.nl, b.jayawardhana@rug.nl, j.d.j.barradas.berglind@rug.nl, j.m.a.scherpen@rug.nl)

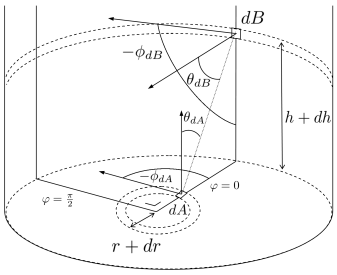

Fig. 1. Graphical interpretation of coordinates used in the Knudsen cosine law and in the remainder of this paper for a cylinder. The considered infinitesimal areas are labeled as dA and dB. Their relative locations are expressed in angles θ and ϕ belonging to each of the infinitesimal areas. Furthermore, φ represents the relative rotation around the central axis of the cylinder.

be used to determine the flux evolution. This evolution of fluxes can be determined through a likeliness function, describing the fractions of particles contained in the flux, that will travel in a corresponding direction once they leave the boundary. The basis for this likeliness function is provided by the Knudsen cosine law [2]. With reference to Fig. 1, where we consider the particle transfer between two infinitesimal surfaces dA and dB, the Knudsen cosine law for the transfer from dA to dB can be stated as

$$p_{dA}(dB) = \frac{\cos(\theta_{dA})\cos(\theta_{dB})}{\mathrm{dist}(dA, dB)^2 \pi} dB, \tag{1}$$

where $p_{dA}(dB)$ is the fraction of particles that leaves an infinitesimal area dA in the direction of dB, θ_{dA} is the angle between the normal of dA and the line connecting dA to dB, θ_{dB} is the angle between the normal of dB and the line connecting dA and dB, and $\mathrm{dist}(dA, dB)$ is the Euclidean distance between dA and dB. Similarly, $P_{dB}(dA)$ can be obtained by replacing dB by dA and vice versa in (1).

The Knudsen cosine law is generally considered to hold well for weakly absorbing and rough surfaces. In this paper, the Knudsen cosine law will serve as the fundamental function describing these transfer fractions. Assuming that it is a static distribution, we can use it to compute constant transfer fractions between discrete space surfaces.

III. Modeling framework for FMF deposition processes

For a given geometry containing a FMF regime, we are interested in the evolution of fluxes over time through a spatial discretization of the inner surface of the geometry. Therefore, we discretize the geometry in n-elements and add an additional flux sink element that has no geometric interpretation. Furthermore, we consider an incoming flux that can be manipulated by a controller. Consequently, we consider the spatially discretized model as follows

$$\dot{x}(t) = (\mathcal{A} + \mathcal{L})x(t) + \mathcal{B}(t)u(t) - \sigma\big(x(t), s(t)\big), \tag{2}$$

$$\dot{s}(t) = \sigma\big(x(t), s(t)\big), \tag{3}$$

$$y(t) = \mathcal{C}\begin{bmatrix} x(t)^\top & s(t)^\top \end{bmatrix}^\top. \tag{4}$$

In (2)-(4), the state $x(t) \in \mathbb{R}^{n+1}$ represents particle fluxes (in particles per second) to discrete surface areas $\{\Omega_1, \Omega_2, ..., \Omega_n\}$ and the sink, $s(t) \in \mathbb{R}^{n+1}$ represents particles that are stuck to the same collection of surfaces as considered for $x(t)$. The matrix $\mathcal{A} \in \mathbb{R}^{n+1 \times n+1}$ describes the particle transfer that is calculated based on the Knudsen cosine law as in (1), between all pairs of the n discrete surfaces, satisfying $\sum_i \mathcal{A}(i,j) = 0$, $\forall j = 1, ..., n+1$. The matrix $\mathcal{L} \in \mathbb{R}^{n+1 \times n+1}$ incorporates the leakage and re-entry of fluxes by allocating them to the sink state and vice versa, satisfying $\sum_i \mathcal{L}(i,j) = 0$, $\forall j = 1, ..., n+1$. The vector $\mathcal{B}(t) \in \mathbb{R}^{n+1 \times m}$ is a time-varying matrix that describes the allocation of controlled input fluxes $u(t) \in \mathbb{R}^m$ to the n discrete surfaces and the sink. The function $\sigma(x(t), s(t))$ is an $(n+1)$-dimensional vector that describes the non-linear adsorption and desorption fractions for each of the n discrete surfaces. The matrix $\mathcal{C} \in \mathbb{R}^{q \times 2(n+1)}$ is the output matrix, relating states to the output $y(t) \in \mathbb{R}^q$. We discuss each component more extensively in the sequel.

A. Transfer matrix $\mathcal{A}$ and leakage matrix $\mathcal{L}$

We can determine the particles transfer matrix $\mathcal{A}$ analytically by calculating the area integration of (1) explicitly, or through an approximation based on numerical integration. The latter can also be realized through sampling/randomization methods. In general, the (i,j)-th element of $\mathcal{A}$ (which corresponds to the particles transfer between discrete surfaces Ω_j and Ω_i) is obtained by solving

$$\mathcal{A}(i,j) = \int_{\Omega_i} \frac{\cos(\theta_{dA})\cos(\theta_{\Omega_j})}{\mathrm{dist}(\Omega_j, dA)^2 \pi} dA - \delta_{ij} \tag{5}$$

where $\delta_{ij} = 1$ if $i = j$ and 0 otherwise. The component δ_{ij} ensures the mass conservation law. We remark that for the simple case where a cylinder is considered and is discretized only along the radius or the height, we have an analytic expression of $\mathcal{A}$ which is presented in [4].

Instead of analytically solving the Knudsen cosine law between different discrete spaces in a given geometry, we can approximate $\mathcal{A}$ through a sampling method, e.g., Monte-Carlo (MC) simulation, as is commonly used in the literature on such processes. In Section V, we compare such an approximation with the analytic computation for the simple cylinder geometry as given in [4] to validate the model.

Note that for approximating the fraction of particles that is transferred between two surfaces, information on the angles between the infinitesimal surfaces θ_{dA} and θ_{dB} (Cf. (1)) is important. Thus, if we consider the illustration in Fig. 1, then we can express the fraction of particle transferred (i.e., the integral in (1)) by the generalized coordinates θ and ϕ. In this case, for setting up the sampling method, we can define the desired density function $F : \left[0, \frac{\pi}{2}\right] \times [0, 2\pi] \to \mathbb{R}_+$ by

$$F(\theta, \phi) = \frac{1}{4\pi} \sin(2\theta) \tag{6}$$

for all $(\theta, \phi) \in \left[0, \frac{\pi}{2}\right] \times [0, 2\pi]$. It can checked that this density function generates the cosine distribution. We can then use MC simulation, with randomness imposed by (6),

to obtain a collection of generalized coordinate pairs (θ, ϕ). These pairs can be allocated to discrete-surfaces through accept-reject algorithms based on the coordinates of the discrete-surface boundaries as expressed in (θ, ϕ) w.r.t. to the considered infinitesimal area. However, we need to obtain the fractions of particles that are exchanged between discrete surfaces. Therefore, for the discrete-surface containing the considered infinitesimal area, we take the average over a sampling of infinitesimal areas belonging to this discrete-surface.

Solving the Knudsen cosine law explicitly yields the most accurate solution, but it quickly becomes non-trivial for finer discretizations or more complex geometries. On the other hand, approximating through sampling remains fairly straightforward for fine discretizations and this approach allows us to deal with more complex geometries encountered in real applications, such as designs of UHV reactors.

Since, in reality, there will always be leakage in such processes, we can easily incorporate the leakage through the use of 'sink' surface. In our modeling formulation in (2), the leakage is encapsulated in the matrix $\mathcal{L}$ and thus, we set the $(n+1)$-th column and row of $\mathcal{A}$ to zero.

B. Incoming flux vector $\mathcal{B}(t)u(t)$

The product of $\mathcal{B}(t)$ and $u(t)$ determines the magnitude and allocation of incoming flux to the discrete surfaces. The input $u(t)$ provides total flux magnitude, while $\mathcal{B}(t)$ allocates this total flux to a collection of discrete surfaces.

C. Sticking function vector $\sigma\big(x(t), s(t)\big)$

The function $\sigma : \mathbb{R}^{n+1} \times \mathbb{R}^{n+1} \mapsto \mathbb{R}^{n+1}$ incorporates the adsorption and desorption phenomena in the flux dynamics. The adsorption, also known as "sticking", is commonly incorporated in the models by means of a sticking coefficient [4]. This coefficient represents the likeliness that a particle, after colliding with a surface, becomes bound to that surface. In addition to the sticking coefficient, we introduce the desorption coefficient, which represents the likeliness that a bound particle leaves a surface. Adding this coefficient has the benefit that we can incorporate reversible adsorption to surfaces in the model. These coefficients are generally dependent on the composition of the local surface and are therefore potentially complicated non-linear functions. A possible form is $\sigma\big(x(t), s(t)\big) = \alpha\big(s(t)\big) \cdot x(t) - \beta\big(s(t)\big) \cdot s(t)$ (for a given constant temperature), where $\alpha(s(t))$ is the sticking coefficient, $\beta(s(t))$ the desorption coefficient and we denote $\cdot$ as element-wise multiplication. When no sticking occurs, we can let $\alpha\big(s(t)\big) = \beta\big(s(t)\big) = 0$.

IV. Point-wise min-norm controller for fluxes in FMF deposition processes

In this section, we discuss a relevant control problem for flux control of a FMF process as modelled by (2)-(4). Flux control is a relevant problem, as for applications like the UHV CVD there can be multi precursors present as a vapour at the same time. The relevant flux intensities (which are like concentrations here) largely influence the obtained reaction equilibria. Note that this can occur while boundaries are saturated and while the requirements for depositions to occur are not met yet (e.g. a reactant is not present yet or the temperature is controlled such that the reactant evaporates quickly). Accordingly, a controller can be designed such that it does not include any sticking.

As FMF processes are typically operated using a pre-determined feed-forward control signal (i.e., the chemical deposition recipes which are typically determined in an empirical setting), hence, robustness and variability are open issues. We will consider these issues while designing a flux controller. In order to achieve robustness and guaranteed performance against uncertainties and variations in the process, we propose a point-wise min-norm controller which takes into account desirable particle flux dynamics w.r.t. relevant surfaces. Ensuring trajectory performance is desired for flux control in FMF as the corresponding systems are typically slow to respond, but very sensitive to fluctuations in reactor conditions.

This requirement of stabilization with guaranteed transient behavior shares the same principle as the stabilization with guaranteed safety as recently proposed in [17]. In order to make this more precise, we let $\mathcal{P} \subset \mathbb{R}^n$ define a closed set around the desired state trajectory x_d, i.e., $x_d(t) \in \mathcal{P}$ for all $t \geq 0$. We also assume that x_d converges to a desired operating point $x^* \in \mathbb{R}^n$. In this case, the problem of stabilization with guaranteed transient behavior for the system in (2)-(4) can be stated as follows.

Stabilization with guaranteed transient behavior problem: For the system in (2)-(4) and given the set $\mathcal{P}$, design a control law $u = k(x)$ such that $x(t) \in \mathcal{P}$ for all t and $x(t) \to x^*$ as $t \to \infty$.

If we consider the complement set of $\mathcal{P}$ as the set of unsafe state $\mathcal{D}$, i.e., $\mathcal{D} = \mathbb{R}^n \backslash \mathcal{P}$, then the above problem can be recast to the stabilization with guaranteed safety problem [17] as given below.

Stabilization with guaranteed safety problem: For the system in (2)-(4) and given the set of unsafe state $\mathcal{D}$, design a control law $u = k(x)$ such that $x(t) \notin \mathcal{D}$ for all t and $x(t) \to x^*$ as $t \to \infty$.

In the sequel, we assume the above dual problem when designing the control law for a FMF process. In the current state-of-the-art, there are mainly two different approaches in solving the stabilization with guaranteed safety problem. The first one is based on the construction of control Lyapunov-Barrier function and the usage of Sontag's universal control law as pursued in [17], [18]; the other one is based on a point-wise min-norm controller, employing both a control Lyapunov function and a control barrier function [19]. As proposed in [17], [18], we can construct the control Lyapunov-Barrier function by combining a control Lyapunov function with a control barrier function, which is not trivial. Since it is not trivial to combine explicitly these functions, we will consider, in this paper, the implementation of the latter approach.

Let us now briefly recall the concept of a control barrier function (CBF) and the point-wise min-norm control formulation as proposed in [19] using quadratic programming. Consider a candidate barrier function $B : \mathbb{R}^n \to \mathbb{R}$ which is $\mathcal{C}^1$ and satisfies

$$\mathcal{D} = \{\xi \in \mathbb{R}^n : B(\xi) \geq 0\}, \tag{7}$$

$$\partial\mathcal{D} = \{\xi \in \mathbb{R}^n : B(\xi) = 0\} \qquad \text{and} \tag{8}$$

$$\mathrm{Int}(\mathcal{D}) = \{\xi \in \mathbb{R}^n : B(\xi) > 0\}. \tag{9}$$

where $\partial\mathcal{D}$ denotes the boundary of $\mathcal{D}$ and $\mathrm{Int}(\mathcal{D})$ denotes the interior of $\mathcal{D}$.

For describing the control Lyapunov function and control barrier function, we need to introduce a few more notations as follows. For a given general affine nonlinear system

$$\dot{x} = f(x) + g(x)u \tag{10}$$

$$y = h(x), \tag{11}$$

with sufficiently smooth functions f, g and h, we denote $L_fV(\xi)$ as the Lie derivative of a function $V : \mathbb{R}^n \to \mathbb{R}$ along the vector field f, i.e., $L_fV(\xi) := \frac{\partial V(\xi)}{\partial \xi} f(\xi)$. Similarly, $L_gV(\xi) := \frac{\partial V(\xi)}{\partial \xi} g(\xi)$. Furthermore, let $U \subset \mathbb{R}^m$ be the set of admissible inputs and $X \subset \mathbb{R}^n$ the set of admissible states.

Exponential safety control barrier function (ES-CBF): A $\mathcal{C}^1$ function $B : \mathbb{R}^n \backslash \mathcal{D} \to \mathbb{R}$ satisfying (7)-(9) is is an ES-CBF if there exist constants $c_1, c_2, c_3, \kappa > 0$ such that

$$-c_1\|\xi\|^2_{\partial\mathcal{D}} - \kappa \leq B(\xi) \leq -c_2\|\xi\|^2_{\partial\mathcal{D}} \tag{12}$$

$$\inf_{v\in U} \left[L_fB(\xi) + L_gB(\xi)v + c_3B(\xi)\right] \leq 0 \tag{13}$$

for all $\xi \in \mathbb{R}^n \backslash \mathcal{D}$, where $\|\xi\|_{\partial\mathcal{D}}$ denotes the shortest Euclidean distance between the point ξ and the boundary of $\mathcal{D}$.

Both conditions of ES-CBF as given above are different to the ones considered in [19], [20], where, in these papers, (12) is replaced by

$$\frac{1}{\alpha_1(\|\xi\|_{\partial\mathcal{D}})} \leq B(\xi) \leq \frac{1}{\alpha_2(\|\xi\|_{\partial\mathcal{D}})}$$

with $\mathcal{K}$ functions α_1, α_2 and (13) is replaced by

$$\inf_{v\in U} \left[L_fB(\xi) + L_gB(\xi)v - \frac{\gamma}{B(\xi)}\right] \leq 0.$$

One can see immediately that the above two conditions are strong ones, in the sense that the corresponding barrier function B has a singularity property at the boundary of $\mathcal{D}$ which may limit the design of B. The use of (12)-(13) has also another nice robustness property, namely, input-to-state safety. We refer the interested reader to [21] for the details on input-to-state safety. Another advantage of assuming (12)-(13) is that we can readily use many numerical tools for polynomials, such as, sum-of-squares, for constructing B.

Similarly, we define an exponential stability control Lyapunov function (ES-CLF) following [19].

Exponential stability control Lyapunov function (ES-CLF): A $\mathcal{C}^1$ function $V : \mathbb{R}^n \mapsto \mathbb{R}$ is an ES-CLF if there exist constants $c_1, c_2, c_3 > 0$ such that

$$c_1\|\xi\|^2 \leq V(\xi) \leq c_2\|\xi\|^2 \tag{14}$$

$$\inf_{v\in U} \left[L_fV(\xi) + L_gV(\xi)v + c_3V(\xi)\right] \leq 0 \tag{15}$$

for all $\xi \in \mathcal{P}$.

For solving the stabilization with guaranteed transient behavior problem w.r.t. the desired set of states $\mathcal{P}$, we will adopt a point-wise min-norm programming using both ES-CLF $V(x)$ and ES-CBF $B(x)$. A review on the design of point-wise min-norm controllers based on ES-CLF for the stabilization of continuous-time nonlinear systems can be found in [22]. We will adopt the point-wise min-norm controller for combining both functions similar to the one pursued in [19], [20].

When we want to combine these two functions, extra care has to be taken since the functionality of ES-CLF and ES-CBF can be conflicting with each other. Indeed, if the inequalities for ES-CBF and ES-CLF hold globally, then the fulfillment of the ES-CBF inequality (c.f., (13)) ensures that the distance to $\mathcal{D}$ grows indefinitely due to (12), which contradicts to the use of ES-CLF that ensures asymptotic convergence of the state to the origin. These two functions can be combined in a domain outside the neighborhood of the origin. In the neighborhood of the origin, the control should be dictated by the ES-CLF. In view of this, in the following discussion, we will partition $\mathcal{P}$ into $\mathcal{P}_{\text{clf\&cbf}}$ and $\mathcal{P}_{\text{clf}}$ such that they overlap and their boundaries are not intersecting with each other.

Point-wise min-norm quadratic program (QP) for stabilization with guaranteed transient behavior.

Let V be an ES-CLF and B be a ES-CBF where $\mathcal{D} = \mathbb{R}^n \backslash \mathcal{P}$. For given constants $\gamma_{\text{clf}}, \gamma_{\text{cbf}} > 0$ and for all $x \in \mathcal{P}_{\text{clf\&cbf}}$, we define the ES-CLBF (Control Lyapunov-Barrier Function) control law $u = k_{\text{clf\&cbf}}(x)$ by the solution of the following QP problem:

$$\textbf{QP1: } k_{\text{clf\&cbf}}(x) = \underset{u}{\operatorname{argmin}} \frac{1}{2}u^\top G(x)u + F(x)^\top u \tag{16}$$

$$\text{s.t.} \begin{cases} L_fV(x) + L_gV(x)u + \gamma_{\text{clf}}V(x) \leq 0, \\ L_fB(x) + L_gB(x)u + \gamma_{\text{cbf}}B(x) \leq 0, \end{cases} \tag{17}$$

where $F, G \succeq 0$ are smooth functions such that $\frac{1}{2}u^\top G(x)u + F(x)^\top u$ is convex. Similarly, for all $x \in \mathcal{P}_{\text{clf}}$, we define the ES-CLF control law $u = k_{\text{clf}}(x)$ by the solution of

$$\textbf{QP2: } k_{\text{clf}}(x) = \underset{u}{\operatorname{argmin}} \frac{1}{2}u^\top G(x)u + F(x)^\top u \tag{18}$$

$$\text{s.t. } L_fV(x) + L_gV(x)u + \gamma_{\text{clf}}V(x) \leq 0. \tag{19}$$

Let $K_{\text{clf}}(\xi)$ define the admissible input set for a given ξ such that the ES-CLF inequality holds, i.e.,

$$K_{\text{clf}}(\xi) := \{v \in U \,|\, L_fV(\xi) + L_gV(\xi)v + \gamma_{\text{clf}}V(\xi) \leq 0\}$$

and similarly, let $K_{\text{cbf}}(\xi)$ define the admissible input set for a given ξ such that the ES-CBF inequality holds, i.e.,

$$K_{\text{cbf}}(\xi) := \{v \in U \mid L_f B(\xi) + L_g B(\xi) v + \gamma_{\text{cbf}} B(\xi) \leq 0\}.$$

Then, we can see that the first necessary and sufficient condition for the feasibility of **QP1** is that

$$K_{\text{clf}}(\xi) \cap K_{\text{cbf}}(\xi) \neq \emptyset \tag{20}$$

holds for all $\xi \in \mathcal{P}_{\text{clf\&cbf}}$.

Another implicit assumption in the feasibility of **QP1** is the Artstein's-like condition for the CLF and the CBF. In this case, we require that for the ES-CLF V, there exists $\gamma_{\text{clf}} > 0$ such that

$$L_f V(\xi) \leq -\gamma_{\text{clf}} V(\xi) \qquad \forall \xi \text{ s.t. } L_g V(\xi) = 0.$$

Similarly, for the ES-CBF B, there exists $\gamma_{\text{cbf}} > 0$ such that

$$L_f B(\xi) \leq -\gamma_{\text{cbf}} B(\xi) \qquad \forall \xi \text{ s.t. } L_g B(\xi) = 0.$$

Based on the ES-CLBF and the ES-CLF control laws, we can propose a simple hybrid automaton controller (as considered also in our previous work in [23]) to stabilize the origin with guaranteed transient behavior as follows. We consider two automata where the domains are given by $\mathcal{P}_{\text{clf\&cbf}}$ and $\mathcal{P}_{\text{clf}}$, while the guards are given by the boundary of $\mathcal{P}_{\text{clf\&cbf}}$ and $\mathcal{P}_{\text{clf}}$, respectively. Depending on the active automaton, we implement either $u = k_{\text{clf\&cbf}}(x)$ or $u = k_{\text{clf}}(x)$. The reset map will be identity, i.e., there is no resetting of state variables. The jump only occurs when the boundary of the active domain is reached, in which case, we switch to the other control law. Since we assume that the domains have overlap with no intersecting boundaries, we ensure that there will be a minimum dwell-time that prevents Zeno behavior to occur.

Theorem 1: The control laws $u = k_{\text{clf\&cbf}}(x)$ and $u = k_{\text{clf}}(x)$ are locally piecewise Lipschitz continuous and the proposed hybrid automata controller solves the problem of stabilization with guaranteed transient behavior.

Proof: The proof of local piecewise Lipschitz continuity follows the same arguments as the proof of Theorem 8 and 11 in [20], which is based on the use of Karush-Kuhn-Tucker condition for optimality to the QP problem with convex cost function and nonlinear affine constraints. In this case, the closed-form of the $k_{\text{clf\&cbf}}(x)$ and $k_{\text{clf}}(x)$ can be expressed as a function of the KKT multipliers and the Lie derivatives of V and B.

For the closed-loop system, from (17) and (19), we have that V satisfies

$$\dot{V}(x(t)) \leq -\gamma_{\text{clf}} V(x)$$

for all $x(t) \in \mathcal{P}$ in both discrete state of automaton. This implies immediately that V is a common Lyapunov function that shows the convergence of x to the origin exponentially. On the other hand, when $x(t) \in \mathcal{P}_{\text{clf\&cbf}}$, we have that B satisfies

$$\dot{B}(x(t)) \leq -\gamma_{\text{cbf}} B(x)$$

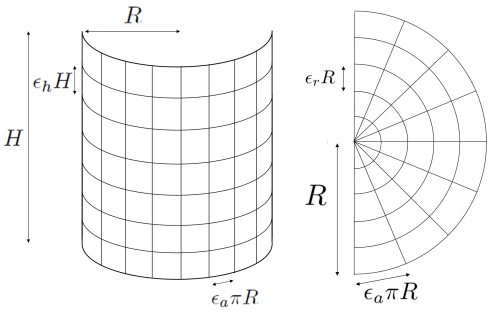

Fig. 2. For our example geometry of a cylinder, we implement a discretization as shown in this figure. By choosing values for ϵ_a, ϵ_r and ϵ_h, we create a uniform grid in two dimensions on the top, side and bottom of the cylinder.

which, together with the lower and upper bound of B, implies that x will never enter $\mathcal{D}$. Therefore, we achieve stabilization with guaranteed transient behavior. ■

V. Numerical example

We consider flux control for a cylindrical reaction chamber with height $H = 10$ and radius $R = 5$. Let us shortly describe the spatial discretization of our cylinder example as shown in Fig. 2. We take $\epsilon_a = \frac{1}{8}, \epsilon_r = \frac{1}{4}$ and $\epsilon_h = \frac{1}{8}$. Accordingly, we define lines along the surfaces of the cylinder, such that these lines act as boundaries for the discrete surfaces. In cylindrical coordinates, the lines span $([0, R], 0, j\epsilon_a \pi)$, $([0, R], H, j\epsilon_a \pi)$ and $(R, [0, H], j\epsilon_a \pi)$, where $j = 0, 1, ..., 2\epsilon_a^{-1}$, for the cylinder bottom, top and side, respectively. The lines in the height dimension on the side of the cylinder then span $(R, q\epsilon_h H, [0, 2\pi])$, where $q = 0, 1, ..., \epsilon_h^{-1}$. The lines in the radial dimension on the bottom and top span $(i\epsilon_r R, 0, [0, 2\pi])$ and $(i\epsilon_r R, H, [0, 2\pi])$, respectively, where $i = 0, 1, ..., \epsilon_r^{-1}$. The number of discrete surface elements is then given by $n = 2\epsilon_h^{-1}\epsilon_a^{-1} + 4\epsilon_r^{-1}\epsilon_a^{-1} = 256$.

As a first step, we need to obtain the matrix $\mathcal{A}$. We use Monte-Carlo simulations to obtain transfer fractions between discrete surfaces, which form matrix $\mathcal{A}$, with the densities of departing angles as in (6). We use the discrete surface boundaries, expressed in the θ and ϕ coordinates with respect to the considered infinitesimal as accept reject conditions. As a next step, we relate an infinitesimal to a discrete area by taking the average transfer fractions of sampled infinitesimal areas belonging to that surface. We have then found the surface-to-surface transfer matrix as computable in the integral part of (5), and are left with subtracting the identity variable δ to obtain $\mathcal{A}$.

A. System model validation

In order to verify our MC simulation results, we make a comparison with the paper of Cale and Raupp [4]. The results of this comparison are shown in Fig. 3.

B. Controller design

As we are dealing with a situation in which no sticking occurs, we have that $\alpha = \beta = \dot{s} = 0$. Also, we assume

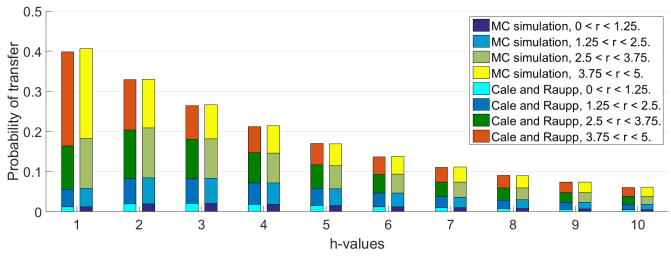

Fig. 3. Results of the MC simulation in comparison with the analytic integration presented by Cale and Raupp in [4]. The comparison is made for several infinitesimal points along the side of the cylinder, whose height values are displayed on the x-axis. The probability shown is given for the four discrete surface rings on the bottom of the cylinder, with values of the radius r spanning the bounds given by the legend.

that fluxes that have escaped our geometry do not re-enter. Therefore, we do not need to explicitly model the sink state and we omit it for convenience of notation; thus, we consider $x \in \mathbb{R}^{256}$ and the state s is neglected. Our goal is to converge to an equilibrium state vector x^* in such a way that we have guaranteed transient behavior, namely $x \in \mathcal{P}$.

Let us shortly describe the remaining system dynamics as in (2)-(4) that we consider. For the leakage matrix $\mathcal{L}$, we consider $\mathcal{L} = -\frac{0.25}{256}\mathbb{1}^{256\times256}$, where $\mathbb{1}^{N\times N}$ is an $N \times N$ matrix whose elements are all one. For the input and measurement vectors $\mathcal{B}$ and $\mathcal{C}$, we assign a value of $\frac{1}{6}$ to two times tree neighbouring elements, located in the 3rd and 4th ring of discrete elements as seen from the centre of the bottom of the cylinder. The locations of $\mathcal{B}$ and $\mathcal{C}$ are then s.t. they are symmetric to each other, where the centre of the bottom of the cylinder is the point of symmetry.

For facilitating the control design where we use a quadratic program formulation, we first obtain a reduced-order model as follows. We reduce the vector of states x from $\mathbb{R}^{256}$ as in (2)-(4) to $\mathbb{R}^2$ through balanced truncation [24] with a maximum $\mathcal{H}_\infty$ norm difference between the two systems of 1.9900×10^{-4}. Let us furthermore incorporate u as a state (with $v := \dot{u} \in \mathbb{R}$, where v is a new input) to obtain a relative degree of 2 which will enable us to design an ES-CBF for shaping both y and $\dot{y}$ as will be discussed later. Hence, the resulting reduced order dynamics with $x \in \mathbb{R}^3$ can be expressed in the canonical observable form as

$$\dot{x} = \bar{A}x + \bar{B}v = \begin{bmatrix} 0 & 0 & 0 \\ 1 & 0 & a_1 \\ 0 & 1 & a_2 \end{bmatrix} x + \begin{bmatrix} b_1 \\ b_2 \\ 0 \end{bmatrix} v, \tag{21}$$

$$y = \bar{C}x = \begin{bmatrix} 0 & 0 & 1 \end{bmatrix} x, \tag{22}$$

with $a_1 = -0.1051, a_2 = -0.5334, b_1 = 5.5067 \times 10^{-5}$ and $b_2 = 3.6872 \times 10^{-4}$. Furthermore, we consider the desired equilibrium as $x^* = \begin{bmatrix} 105 & 533 & 1000 \end{bmatrix}^\top$.

Subsequently, to facilitate the implementation of the point-wise min-norm control with guaranteed transient behavior for the reduced-order model in (21)-(22) we consider our candidate ES-CLF as follows

$$V(x - x^*) = \frac{1}{2}(x - x^*)^\top (x - x^*), \tag{23}$$

such that the corresponding constraint to the ES-CLF in (17) becomes

$$\frac{\partial V(x - x^*)}{\partial x}(\bar{A}x + \bar{B}v) \leq -\gamma_{\text{clf}} V(x - x^*). \tag{24}$$

Furthermore, we consider an ES-CBF candidate which will effectively prevent the measured output $y = x_3$ from growing rapidly by providing an upper limit for $\dot{y} = x_2 + a_2 x_3$. This ES-CBF candidate is then described by

$$B(x) = -\frac{(x_3 - 100)^2}{600} - \left(x_2 + a_2 x_3 - 115\right)^2 + 100^2, \tag{25}$$

in terms of x_2 and x_3, such that (25) contains the set of the unsafe states $\mathcal{D}$ and has the desired effect of providing a maximum for $\dot{y}$. Hence, the corresponding constraint to the ES-CBF in (17) yields

$$\frac{\partial B(x)}{\partial x}(\bar{A}x + \bar{B}v) \leq -\gamma_{\text{cbf}} B(x) \tag{26}$$

and is providing the desired transient behavior guarantees.

Let us now define the two domains and guards for the two automata. For the ES-CLBF automaton, we choose $\mathcal{P}_{\text{clf\&cbf}} = \{x | \dot{y} > 8\} = \{x_2, x_3 | x_2 + a_2 x_3 > 8\}$ with guard condition $\dot{y} \leq 8$. For the ES-CLF automaton, we choose $\mathcal{P}_{\text{clf}} = \{x | \dot{y} < 9\}$ with guard condition $\dot{y} \geq 9$. Consequently, combining (24) and (26), we obtain the ES-CLBF for the stabilizing flux controller with guaranteed transient behavior for the reduced order FMF process in (21) - (22) by solving the realization of (16) - (19) for this example, given by

$$\textbf{QP1e: } k_{\text{clf\&cbf}}(x) = \arg\min_v v^\top G(x) v + F(x)^\top v \tag{27}$$

$$\text{s.t. } \begin{cases} \frac{\partial V(x-x^*)}{\partial x}(\bar{A}x + \bar{B}v) \leq -\gamma_{\text{clf}} V(x - x^*), \\ \frac{\partial B(x)}{\partial x}(\bar{A}x + \bar{B}v) \leq -\gamma_{\text{cbf}} B(x), \end{cases} \tag{28}$$

for the ES-CLBF automaton and

$$\textbf{QP2e: } k_{\text{clf}}(x) = \arg\min_v v^\top G(x) v + F(x)^\top v \tag{29}$$

$$\text{s.t. } \frac{\partial V(x - x^*)}{\partial x}(\bar{A}x + \bar{B}v) \leq -\gamma_{\text{clf}} V(x - x^*), \tag{30}$$

for the ES-CLF automaton. Furthermore, we let $\gamma_{\text{clf}} = 0.03$ and $\gamma_{\text{cbf}} = 100$, $G(x) = 1$, and $F(x)$ be a convex combination of the ES-CLF and the ES-CBF, such that the trajectories avoid the boundaries. The simulation results are presented in the sequel.

C. Simulation results and discussion

We implement the control design from section V.A to the original full-order system. The performance of the controlled system can be observed in the y-$\dot{y}$ plane shown in Fig. 4 and in the output trajectory depicted in Fig. 5. We have compared the performance of a controller that utilizes solely the ES-CLF control law with a controller that utilizes both the ES-CLF and the ES-CLBF control laws, for **QP1e** (27)-(28) and **QP2e** (29)-(30). While the former achieves the stabilization goals, the latter achieves better convergence speed performance. The ES-CLF alone could not achieve a similar convergence speed without becoming unsafe. Furthermore, the ES-CBF will always prevent the system trajectory from

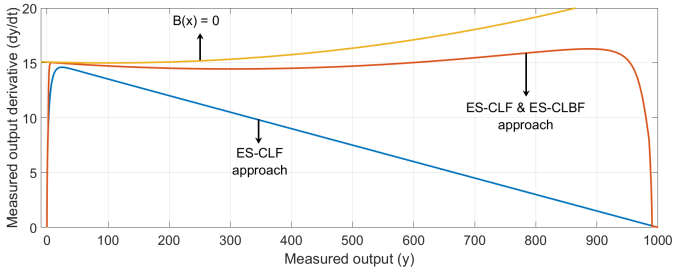

Fig. 4. Controlled system performance in terms of $y(= x_3)$ and $\dot{y}(= x_2 + a_2 x_3)$, for **QP1e** and **QP2e** given by (27)-(30). For the ES-CLF approach, the only control law used is the ES-CLF. For the ES-CLF & ES-CLBF approach, both the ES-CLF and the ES-CLBF control laws are used. $B(x) = 0$ is the plot of the barrier function B (equal to zero).

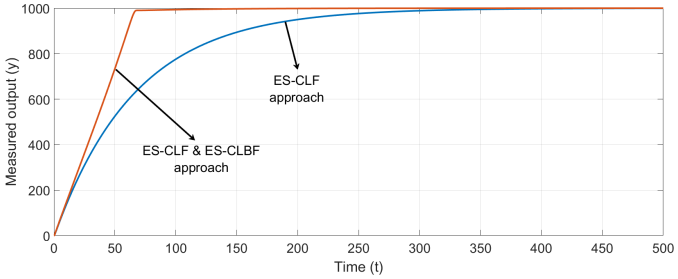

Fig. 5. Controlled system performance in terms of $y(t)$ for **QP1e** and **QP2e** given by (27)-(30). For the ES-CLF approach, the only control law used is the ES-CLF. For the ES-CLF & ES-CLBF approach, both the ES-CLF and the ES-CLBF control laws are used.

becoming unsafe, since it guarantees that the solution of **QP1e** in (27)-(28) becomes in-feasible due to violation of condition (20) if a trajectory should enter the unsafe set.

VI. Conclusions

In this paper, we presented a modeling framework for FMF deposition processes, which is suitable for model-based control design. Furthermore, we proposed a point-wise min-norm control design method for stabilization with guaranteed transient behavior for fluxes. The proposed strategy is given by a simple hybrid automata controller, based on a control Lyapunov function control law and a control Lyapunov-barrier function control law. We validated our modeling framework against existing results in the literature for a cylindrical geometry. Lastly, the applicability of both the modeling framework and the control strategy with guaranteed stabilization and transient behavior for fluxes were illustrated by simulation results for a reduced order FMF process in a cylindrical geometry.

References

[1] M. Knudsen, "Die gesetze der molekularstrmung und der inneren reibungsstrmung der gase durch rhren," *Annalen der Physik*, vol. 28, pp. 75–130, 1909.

[2] ——, "The cosine law in the kinetic theory of gases," *Annalen der Physik*, vol. 48, pp. 1113–1121, 1915.

[3] W. Steckelmacher, "Knudsen flow 75 years on: The current state of the art for flow of rarefied gases in tubes and systems," *Reports on Progress in Physics*, vol. 49, pp. 1083–1107, 1986.

[4] T. Cale and G. Raupp, "Free molecular transport and deposition in cylindrical features," *Journal of Vacuum Science & Technology B: Microelectronics Processing and Phenomena*, vol. 8, no. 4, pp. 649–655, 1990.

[5] R. Dorsman, C. R. Kleijn, J. F. M. Velthuis, J. P. Zijp, and A. M. B. V. Mol, "Zinc deposition experiments for validation of direct-simulation Monte Carlo calculations of rarefied internal gas flows," *Journal of Vacuum Science Technology A*, vol. 25, no. 3, 2007.

[6] R. A. Adomaitis, "A ballistic transport and surface reaction model for simulating atomic layer deposition processes in high-aspect-ratio nanopores," *Chemical Vapor Deposition*, vol. 17, no. 10-12, pp. 353–365, 2011.

[7] A. Holmqvist, T. Törndahl, and S. Stenström, "A model-based methodology for the analysis and design of atomic layer deposition processes - Part I: Mechanistic modelling of continuous flow reactors," *Chemical Engineering Science*, vol. 81, pp. 260–272, 2012.

[8] R. G. Gordon, D. Hausmann, E. Kim, and J. Shepard, "A kinetic model for step coverage by atomic layer deposition in narrow holes or trenches," *Chemical Vapor Deposition*, vol. 9, no. 2, 2003.

[9] S. Villani, *Isotope separation*. Amer Nuclear Society, 1976.

[10] A. Kogan, "Direct solar thermal splitting of water and on-site separation of the products II. Experimental feasibility study," *International Journal of Hydrogen Energy*, vol. 23, no. 2, pp. 89–98, 1998.

[11] V. Calabro, B. L. Jiao, and E. Drioli, "Theoretical and experimental study on membrane distillation in the concentration of orange juice," *Industrial & engineering chemistry research*, vol. 33, no. 7, pp. 1803–1808, 1994.

[12] F. Sharipov and V. Seleznev, "Data on internal rarefied gas flows," *Journal of Physical and Chemical Reference Data*, vol. 27, no. 3, pp. 657–706, 1998.

[13] Y. Shi, Y. T. Lee, and A. S. Kim, "Knudsen diffusion through cylindrical tubes of varying radii: theory and Monte Carlo simulations," *Transport in porous media*, vol. 93, no. 3, pp. 517–541, 2012.

[14] T. F. Edgar, S. W. Butler, W. J. Campbell, C. Pfeiffer, C. Bode, S. B. Hwang, K. Balakrishnan, and J. Hahn, "Automatic control in microelectronics manufacturing: Practices, challenges, and possibilities," *Automatica*, vol. 36, no. 11, pp. 1567–1603, 2000.

[15] A. Holmqvist, T. Törndahl, and S. Stenström, "A model-based methodology for the analysis and design of atomic layer deposition processes - Part II: Experimental validation and mechanistic analysis," *Chemical Engineering Science*, vol. 94, pp. 316–329, 2013.

[16] ——, "A model-based methodology for the analysis and design of atomic layer deposition processes - Part III: Constrained multi-objective optimization," *Chemical Engineering Science*, vol. 96, pp. 71–86, 2013.

[17] M. Z. Romdlony and B. Jayawardhana, "Stabilization with guaranteed safety using Control Lyapunov-Barrier function," *Automatica*, vol. 66, pp. 39–47, 2016.

[18] ——, "Uniting control Lyapunov and control barrier functions," in *Proceedings of the 53rd IEEE Conference on Decision and Control*. IEEE, 2014, pp. 2293–2298.

[19] A. D. Ames, J. W. Grizzle, and P. Tabuada, "Control barrier function based quadratic programs with application to adaptive cruise control," in *Proceedings of the 53rd IEEE Conference on Decision and Control*. IEEE, 2014, pp. 6271–6278.

[20] X. Xu, P. Tabuada, J. W. Grizzle, and A. D. Ames, "Robustness of control barrier functions for safety critical control," *IFAC-PapersOnLine*, vol. 48, no. 27, pp. 54–61, 2015.

[21] M. Z. Romdlony and B. Jayawardhana, "On the new notion of input-to-state safety," in *Proceedings of the 55th IEEE Conference on Decision and Control*. IEEE, 2016, pp. 6403–6409.

[22] J. A. Primbs, V. Nevistić, and J. C. Doyle, "Nonlinear optimal control: A control Lyapunov function and receding horizon perspective," *Asian Journal of Control*, vol. 1, no. 1, pp. 14–24, 1999.

[23] M. Z. Romdlony and B. Jayawardhana, "Passivity-based control with guaranteed safety via interconnection and damping assignment," *IFAC-PapersOnLine*, vol. 48, no. 27, pp. 74 – 79, 2015.

[24] A. C. Antoulas, *Approximation of large-scale dynamical systems*. Siam, 2005.